

 Open access • Journal Article • DOI:10.1063/1.3621835





Influence of the Cu-Te composition and microstructure on the resistive switching of Cu-Te/Al₂O₃/Si cells — [Source link](#)

Ludovic Goux, Karl Opsomer, Robin Degraeve, Robert Muller ...+5 more authors

Published on: 01 Aug 2011 - Applied Physics Letters (American Institute of Physics)

Related papers:

- [Redox-Based Resistive Switching Memories – Nanoionic Mechanisms, Prospects, and Challenges](#)
- [Nanoionics-based resistive switching memories](#)
- [Electrochemical metallization memories—fundamentals, applications, prospects](#)
- [Observation of conducting filament growth in nanoscale resistive memories](#)
- [Electrochemical dynamics of nanoscale metallic inclusions in dielectrics](#)

Share this paper:    

View more about this paper here: <https://typeset.io/papers/influence-of-the-cu-te-composition-and-microstructure-on-the-1kr3en43b8>

Influence of the Cu-Te composition and microstructure on the resistive switching of Cu-Te/Al₂O₃/Si cells

L. Goux, K. Opsomer, R. Degraeve, R. Müller, C. Detavernier et al.

Citation: *Appl. Phys. Lett.* **99**, 053502 (2011); doi: 10.1063/1.3621835

View online: <http://dx.doi.org/10.1063/1.3621835>

View Table of Contents: <http://apl.aip.org/resource/1/APPLAB/v99/i5>

Published by the [American Institute of Physics](#).

Related Articles

Kelvin probe force gradient microscopy of charge dissipation in nano thin dielectric layers

J. Appl. Phys. **110**, 084304 (2011)

Kelvin probe study on formation of electric dipole at direct-contact HfO₂/Si interfaces

J. Appl. Phys. **110**, 074115 (2011)

Insight into unusual impurity absorbability of GeO₂ in GeO₂/Ge stacks

Appl. Phys. Lett. **99**, 142101 (2011)

Electrical properties of atomic layer deposited aluminum oxide on gallium nitride

Appl. Phys. Lett. **99**, 133503 (2011)

Characterization of channel strain evolution upon the silicidation of recessed source/drain Si_{1-x}Ge_x structures

Appl. Phys. Lett. **99**, 133107 (2011)

Additional information on *Appl. Phys. Lett.*

Journal Homepage: <http://apl.aip.org/>

Journal Information: http://apl.aip.org/about/about_the_journal

Top downloads: http://apl.aip.org/features/most_downloaded

Information for Authors: <http://apl.aip.org/authors>

ADVERTISEMENT

AIPAdvances

Submit Now

**Explore AIP's new
open-access journal**

- **Article-level metrics
now available**
- **Join the conversation!
Rate & comment on articles**

Influence of the Cu-Te composition and microstructure on the resistive switching of Cu-Te/Al₂O₃/Si cells

L. Goux,^{1,a)} K. Opsomer,¹ R. Degraeve,¹ R. Müller,¹ C. Detavernier,² D. J. Wouters,¹ M. Jurczak,¹ L. Altimime,¹ and J. A. Kittl¹

¹IMEC, Kapeldreef 75, 3001 Leuven, Belgium

²Universiteit Gent, Krijgslaan 281 (S1), 9000 Gent, Belgium

(Received 10 May 2011; accepted 13 July 2011; published online 1 August 2011)

In this letter, we explore the influence of the Cu_xTe_{1-x} layer composition ($0.2 < x < 0.8$) on the resistive switching of Cu_xTe_{1-x}/Al₂O₃/Si cells. While $x > 0.7$ leads to large reset power, similar to pure-Cu electrodes, $x < 0.3$ results in volatile forming properties. The intermediate range $0.5 < x < 0.7$ shows optimum memory properties, featuring improved control of filament programming using $< 5 \mu\text{A}$ as well as state stability at 85 °C. The composition-dependent programming control and filament stability are closely associated with the phases in the Cu_xTe_{1-x} layer and are explained as related to the chemical affinity between Cu and Te. © 2011 American Institute of Physics. [doi:10.1063/1.3621835]

Resistive Random Access Memory (RRAM) technology has drawn a lot of attention these last years due to scaling potential. Between the different RRAM concepts, the Conducting-Bridging RAM (CBRAM) was demonstrated to show attractive properties, such as endurance robustness and multi-level capability.^{1,2} A CBRAM cell typically consists of a cation-supply electrode, usually based on Cu or Ag metal, an insulating layer serving as electrolyte for metal-cation drift, and an electrochemically inert electrode. A positive electrical potential applied to the former electrode results in the filament growth from the cathode towards the cation-supply electrode, bridging eventually the two electrodes and leading thus to the electrical switching to a low-resistive state (LRS). On the other hand, a negative potential induces the reverse redox reaction, i.e., the filament dissolution and cation drift back towards the cation-supply electrode, accounting in turn for the return to a high-resistive state (HRS).

While chalcogenide materials like GeSe or GeS were originally developed as electrolyte layers,^{1,2} binary-oxide media like HfO₂,³ ZrO₂,⁴ or Ta₂O₅ (Ref. 5) were more recently introduced. Combined with a pure-Cu supply layer, oxide-based CBRAM cells typically exhibit attractive switching properties and filament stability, however they usually require larger reset current I_{RESET} ³⁻⁵ than chalcogenide-based CBRAM cells. On the other hand, the Cu-Te alloy has also recently been introduced as a Cu-supply layer.⁶

In this work, we explore the effect of the Cu_xTe_{1-x} composition on the switching characteristics of an original and integration-friendly Cu_xTe_{1-x}/Al₂O₃/Si cell. We particularly show that the composition range $0.5 < x < 0.7$ results in controlled filament generation and optimized memory characteristics.

A 3 nm-thick Al₂O₃ layer was deposited on doped-Si wafers by an H₂O-based Atomic Layer Deposition (ALD) technique. Then, 3 mm-wide and 50 nm-thick Cu_xTe_{1-x} dots were deposited through a shadow mask by a co-sputtering

process from a Cu target and a Cu_{0.1}Te_{0.9} target. Finally, 1 mm-wide Pt dots were sputtered on top of the Cu_xTe_{1-x} dots using a different shadow mask. Fig. 1(a) shows schematics of the cells.

A combinatorial approach was used to study the effect of Cu_xTe_{1-x} composition. During the co-sputtering process of the Cu_xTe_{1-x} layer, triangular masks placed in front of the sputtering targets result in a composition gradient in the deposited film, with a gradual variation of x along a direction of the wafer, called y -direction hereafter. Fig. 1(b) shows the composition of the Cu_xTe_{1-x} layer determined by X-ray fluorescence (XRF) spectroscopy for each position along the y -direction. Using the 4-point probing method, we verified that the Cu_xTe_{1-x} layer exhibits low resistivity in the whole composition range [Fig. 1(c)].

The Pt/Cu_xTe_{1-x}/Al₂O₃/Si cells were electrically tested using a conventional parameter analyzer HP4156. No load resistor was used. Current-Voltage (I - V) characterization was carried out by applying positive voltage to the Pt top-electrode (TE) for forming and set operations, and negative voltage for reset operation, in agreement with CBRAM switching mode. Note that no switching is obtained when forming is performed using negative voltage ramps.

Fig. 2(a) shows the initial resistance R_{INIT} of the as-prepared cells together with the forming voltage V_F as a function of x in Cu_xTe_{1-x}. On the one hand, R_{INIT} steadily decreases with the increase of x , suggesting enhanced Cu interdiffusion in the Al₂O₃ layer for larger x . On the other hand, V_F shows a strong drop for $x > 0.7$. The X-ray diffraction (XRD) patterns performed on the Cu_xTe_{1-x} layers [Fig. 2(b)] clearly show different microstructures depending on the composition. The Cu_xTe_{1-x} layers are amorphous for $x < 0.5$. XRD peaks corresponding to crystalline Cu-Te phases are identified for $x > 0.5$, while peaks corresponding to crystalline Cu become clearly visible only for $x > 0.7$. These results are in agreement with the Cu-Te phase diagram.⁷⁻⁹ The composition range $x > 0.7$ also showed a marked difference of surface morphology compared to $0.5 < x < 0.7$. Large protrusions, presumably associated with

^{a)}Electronic mail: gouxl@imec.be

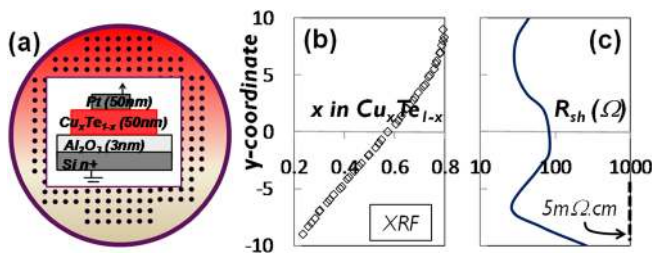


FIG. 1. (Color online) (a) $\text{Cu}_x\text{Te}_{1-x}$ dot pattern on the wafer, the inset showing a schematic cross-section of the cell stack; (b) and (c) relations between the y-coordinate of the cell and the composition and sheet resistance R_{sh} , respectively, of the $\text{Cu}_x\text{Te}_{1-x}$ layer.

the presence of the pure Cu cubic phase, were indeed observed in the range $x > 0.7$ [Fig. 2(c)]. Hence, the drop of V_F for $x > 0.7$ may be associated to the presence of the Cu cubic phase in the Cu-Te layer. This result is in agreement with a recent report showing shorter time to dielectric breakdown for dielectrics having Cu gates instead of electrochemically inert Pt gates.⁵

The $\text{Cu}_x\text{Te}_{1-x}$ composition also strongly affects subsequent resistive switching, in particular the filament characteristics. Figs. 3(a) and 3(b) show, respectively, the LRS resistance R_{LRS} and the reset current I_{RESET} extracted from negative voltage ramps performed after set switching operations using the compliance currents $I_{COMP} = 100 \mu\text{A}$ or $I_{COMP} = 5 \mu\text{A}$. Larger I_{COMP} leads to lower R_{LRS} and larger I_{RESET} , as widely reported in the literature for RRAM (Ref. 10) and CBRAM (Refs. 11 and 12) devices. In addition, three main composition regions may be distinguished, associated with the typical $I-V$ traces shown in Fig. 3(c). For region (1) $x < 0.5$, very unstable Cu filament is generated [Figs. 3(a) and 3(b)], and the lower x values typically result in volatile forming characteristics [Fig. 3(c)], which may

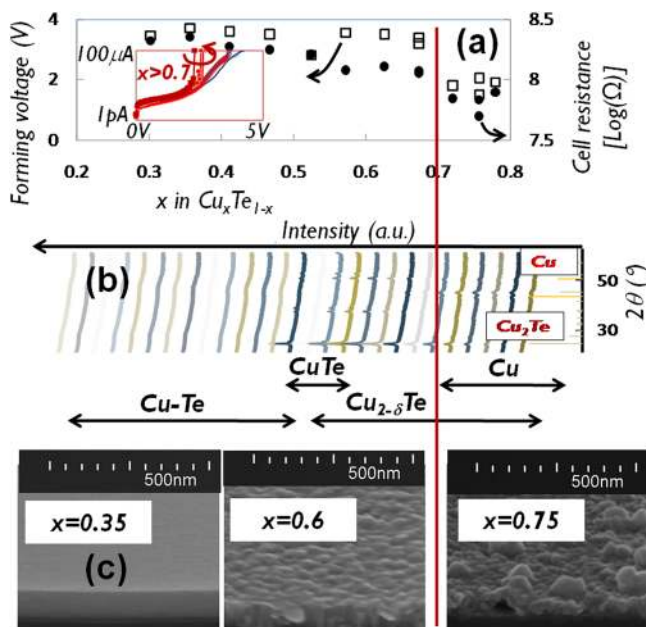


FIG. 2. (Color online) (a) Forming voltage V_F and resistance R_{INIT} of as-prepared cells (measured at $+0.2\text{V}$) as a function of x in $\text{Cu}_x\text{Te}_{1-x}$; the inset shows the forming $I-V$ traces; (b) XRD diagrams of the $\text{Cu}_x\text{Te}_{1-x}$ layers, revealing different phases depending on the x range; (c) Scanning Electron Microscopy (SEM) images showing the surface morphologies of the $\text{Cu}_x\text{Te}_{1-x}$ layer for different x values.

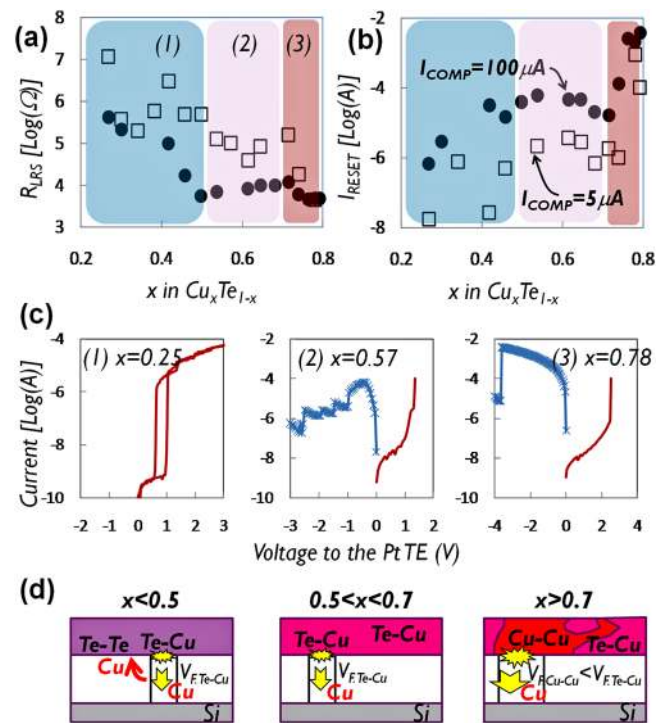


FIG. 3. (Color online) LRS resistance R_{LRS} (a) and reset current I_{RESET} (b) as a function of x in $\text{Cu}_x\text{Te}_{1-x}$, both extracted after set switching using $I_{COMP} = 100 \mu\text{A}$ (full circles) or $I_{COMP} = 5 \mu\text{A}$ (empty squares); (c) Typical $I-V$ set and reset traces observed for the three composition regions (1) $x < 0.5$, (2) $0.5 < x < 0.7$, and (3) $x > 0.7$; (d) Schematics of the phenomenology of Cu-filament formation in each region.

appear attractive for diode-selector applications. For region (3) $x > 0.7$, a stable Cu filament is formed, however requiring large reset current $I_{RESET} \gg I_{COMP}$, similar to pure-Cu supply layers.³⁻⁵ We also verified this effect by using pure-Cu dots instead of Cu-Te material (not shown here). $I-V$ cycling tests performed in region (3) resulted in $>10\%$ switching failures, probably related to large switching power. On the other hand, region (2) $0.5 < x < 0.7$ shows attractive switching control using low operation current $I_{RESET} \sim I_{COMP}$. Fig. 4(a) confirms the remarkable resistance stability observed in region (2) over 10^3 $I-V$ cycles using $<5 \mu\text{A}$. Filament stability in region (2) is also assessed up to more than 10^4 s at 85°C [Fig. 4(b)]. Similar retention was obtained in region (3).

Hence, the composition range $0.5 < x < 0.7$ in $\text{Cu}_x\text{Te}_{1-x}$ appears as the best trade-off in terms of programming control, limited operation current, and filament stability. The good control of low I_{RESET} by I_{COMP} suggests very little

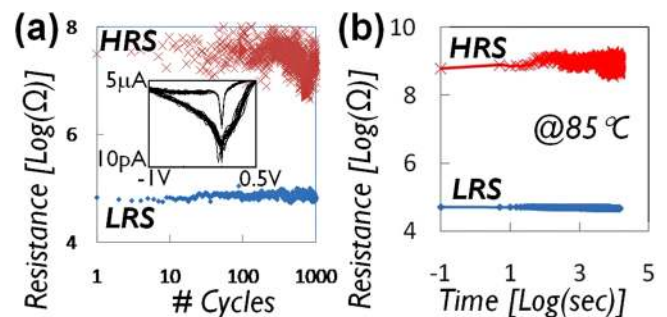


FIG. 4. (Color online) (a) HRS and LRS resistance control observed over 10^3 $I-V$ cycles using $I_{COMP} = 5 \mu\text{A}$ (inset shows 30 consecutive $I-V$ cycles); (b) HRS and LRS resistance monitoring at 85°C using constant bias voltage of 20mV .

sensitivity to the parasitic current overshoot induced by forming/set.¹⁰ We attribute this property to the larger energy barrier for Cu injection from Cu-Te crystal phases compared to pure Cu, due to larger Cu-Te bonding energy. In agreement, Da Silva *et al.* reported density-functional-theory calculations showing that in this composition range the formation energy of Cu-Te structures is lower than the formation energy of pure Cu phase.⁷ Therefore, the Cu injection into the Al₂O₃ layer requires less energy from the Cu cubic phase, which results in a lower V_F values measured for $x > 0.7$ [see inset of Fig. 2(a)]. This also accounts for an increased sensitivity of the cell to discharge current in this range, leading to large Cu electromigration and resulting in overgrown filaments which will require larger I_{RESET} . On the other hand, for $x < 0.5$, the better stability of CuTe and Te phases^{8,9} probably does not allow any stable Cu phase formation, so that the Cu atoms injected at forming will readily diffuse back to the supply layer after power switch off. To the contrary, the stability of Cu filaments for $0.5 < x < 0.7$ may be explained by the stability of Cu-deficient Cu_{2- δ} Te phases in this range [Fig. 2(b)]. Note that the decrease of R_{INT} already observed in this range might also originate from enhanced mobility of Cu in this range.⁷ Fig. 3(d) shows schematics of the filament formation scenario in each region.

To summarize, we showed the strong influence of x in the Cu _{x} Te_{1- x} layer on the memory properties of Cu-Te/Al₂O₃/Si cells, and we associated this influence to the different Cu-Te phase stability regions. Improved control of the filament formation is obtained in the range $0.5 < x < 0.7$ compared to $x > 0.7$, which we attribute to the Cu-Te bonding energy of the phases in the former range. The cell is

programmed using $< 5 \mu\text{A}$ current level without transistor-based current limiter, excellent stability of programming parameters is demonstrated over 10^3 cycles, and state stability was verified up to 10^4 s at 85 °C.

The authors thank P. Hendrickx and R. Schuitema for measurement support and the partial funding by IMEC's Industrial Affiliation program on RRAM.

- ¹M. N. Kozicki, M. Park, and M. Mitkova, *IEEE Trans. Nanotechnol.* **2**, 331 (2005).
- ²M. Kund, G. Beitel, C.-U. Pinnow, T. Röhr, J. Schumann, R. Symanczyk, K.-D. Ufert, and G. Müller, *Tech. Dig. - Int. Electron Devices Meet.* **2005**, 754.
- ³Y. Wang, H. Lv, W. Wang, Q. Liu, S. Long, Q. Wang, Z. Huo, S. Zhang, Y. Li, Q. Zuo, W. Lian, J. Yang, and M. Liu, *Electron Device Lett.* **31**(12), 1470 (2010).
- ⁴Q. Liu, S. Long, W. Wang, Q. Zuo, S. Zhang, J. Chen, and M. Liu, *Electron Device Lett.* **30**(12), 1335 (2009).
- ⁵T. Tsuruoka, K. Terabe, T. Hasegawa, and M. Aono, *Nanotechnology* **21**, 425205 (2010).
- ⁶K. Aratani, K. Ohba, T. Mizuguchi, S. Yasuda, T. Shiimoto, T. Tsushima, T. Sone, K. Endo, A. Kouchiyama, S. Sasaki, A. Maesaka, N. Yamada, and H. Narisawa, *Tech. Dig. - Int. Electron Devices Meet.* **2005**, 783.
- ⁷J. L. F. Da Silva, S.-H. Wei, J. Zhou, and X. Wu, *Appl. Phys. Lett.* **91**, 091902 (2007).
- ⁸P. F. Carcia, F. D. Kalk, P. E. Bierstedt, A. Ferretti, G. A. Jones, and D. G. Swartzfager, *J. Appl. Phys.* **64**(4), 1671 (1988).
- ⁹S. K. Chattopadhyay, S. K. Chatterjeet, and S. P. Sen Gupta, *J. Phys. D: Appl. Phys.* **22**, 142 (1989).
- ¹⁰L. Goux, J. G. Lisoni, X.P. Wang, M. Jurczak, and D. J. Wouters, *IEEE Trans. Electron Devices* **56**(10), 2363 (2009).
- ¹¹C. Schindler, S. C. P. Thermadam, R. Waser, and M. N. Kozicki, *IEEE Trans. Electron Devices*, **54**(10), 2762 (2007).
- ¹²U. Russo, D. Kamalanathan, D. Ielmini, A. L. Lacaita, and M. N. Kozicki, *IEEE Trans. Electron Devices* **56**(5), 1040 (2009).